A spectroscopic study of mechanochemically activated kaolinite with the aid of chemometrics

Onuma Carmody[1a], János Kristóf[b], Ray L. Frost[a], Éva Makó[c], J. Theo Kloprogge[a], and Serge Kokot[a].

[a]*Inorganic Materials Research Program, Queensland University of Technology, Brisbane, Queensland, Australia.*
[b]*Department of Analytical Chemistry, University of Veszprem, Veszprem, Hungary*
[c]*Department of Silicate and Materials Engineering, University of Veszprem, Veszprem, Hungary*

Frost, Ray and Carmody, Onuma and Kristof, Janos and Kokot, Serge and Kloprogge, Theo (2005) A spectroscopic study of mechanochemically activated kaolinite with the aid of chemometrics. . *Journal of Colloid and Interface Science* 287(1):43-56.

Abstract

The study of kaolinite surfaces is of industrial importance. In this work we report the application of chemometrics to the study of modified kaolinite surfaces. DRIFT spectra of mechanochemically activated kaolinites (Kiralhegy, Zettlitz, Szegi and Birdwood) were analysed using, Principal Component Analysis (PCA), and multi-criteria decision making (MCDM) methods, PROMETHEE and GAIA. The clear discrimination of the Kiralhegy spectral objects on the two PC scores plots (400-800 and 800-2030 cm^{-1}) indicated the dominance of quartz. Importantly, no ordering of any spectral objects appeared to be related to grinding time in the PC plots of these spectral regions. Thus, neither the kaolinite nor the quartz, are systematically responsive to grinding time according to the spectral criteria investigated. The third spectral region (2600-3800 cm^{-1} – OH vibrations), showed apparent systematic ordering of the Kiralhegy and, to a lesser extent, Zettlitz spectral objects with grinding time. This was attributed to the effect of the natural quartz on the delamination of kaolinite and the accompanying phenomena (i.e. formation of kaolinite spheres and water). With the MCDM methods, it was shown that useful information on the basis of chemical composition, physical properties and grinding time can be obtained. For example, the effects of the minor chemical components (e.g. MgO, K_2O etc) indicated that the Birdwood kaolinite is arguably the most pure one analysed. In another MCDM experiment, some support was obtained for the apparent trend with grinding time noted in the PC plot of the OH spectral region.

Keywords: kaolinite surfaces, chemometrics, PCA, PROMETHEE and GAIA, DRIFT

---

[1] Corresponding author.
Email address: o.carmody@student.qut.edu.au
Address: 2 George Street, Brisbane Q 4001, Australia

1 Introduction

Kaolinite is one of the most important clay minerals and has wide industrial applications. It is used in the production of ceramics and porcelain, and as a filler for paint, rubber and plastics [1, 2]. However, the greatest demand for kaolinite is in the paper industry where it is used to produce glossy paper such as those in magazines [3]. The wide industrial application of kaolinite depends on the ability to modify its properties for other uses. One such method is the mechanochemical activation of kaolinite through dry or wet grinding. Other methods used to modify kaolinite surfaces include intercalation and thermal treatment [4-6].

Studies have been undertaken to investigate changes in the kaolinite structure due to grinding over a long period of time [7-13]. Various techniques that have been used to study changes in kaolinite include X-ray diffraction, infrared spectroscopy, thermal analysis, electron microscopy, and Raman spectroscopy. Laws and Page [14] studied changes arising from grinding of the kaolinite and some aspects of the resulting product. Schrader [15] comprehensively studied the mechanochemical transformation of the kaolinite structure and observed that increased grinding causes the crystal structure to deform mainly along the *c* axis with the crystal structure along the *b* axis proving to be more resistant (i.e. deformation between the layers but not within the layers). In addition, increased grinding decreased crystallite size significantly along the *c* axis, and slightly along the *b* axis, causing the kaolinite structure to delaminate. Takahashi [7] and Kohler et al. [16] found that prolonged dry grinding (over 36 hours) resulted in a disordered phase which yielded an amorphous material due to the complete destruction of the kaolinite structure. The gradual destruction of kaolinite affects its physical and chemical properties including particle size [11, 12], specific surface area [12, 16], cation exchange capacity [17, 18], water absorption capability and energy [19, 20], acid solubility [17] and aggregate formation [21].

Mechanochemical activation as studied by Scanning Electron Microscopy (SEM) and Transmission Electron Microscopy (TEM) shows the disintegration, aggregation and agglomeration of the kaolinite [12, 21]. It was found that dry grinding causes the kaolinite layers to fragment and results in the formation of spheroidal particles. According to Juhasz [12], these spheroidal particles result from the mechanochemical activation process where grinding causes a) initial increase in the degree of dispersion; b) aggregate formation due to interpartial adhesion; c) aggregate compaction (agglomeration) due to the effect of high surface forces; and d) dispersion of aggregates at a sufficient degree of compactness.

Infrared spectroscopy has also been used to study the changes in the molecular structure of kaolinite during grinding [22]. The structural alterations characterised by X-ray diffraction measurements are supported by various studies with infrared spectroscopy. According to Farmer [23], kaolinite hydroxyl groups have four infrared stretching bands. The bands are assigned in accordance with the inner surface hydroxyls (3695, 3670 and 3650 cm^{-1}) and inner hydroxyls (3620 cm^{-1}). Thus, structural changes as the result of grinding are reflected in the infrared spectra of the hydroxyl stretching region. With the use of infrared spectra, Miller and Oulton [24] observed a deterioration of the kaolinite structure and explained the removal of protons from inner surface and inner hydroxyls. Frost et al. [25, 26] and Gonzalez Garcia et al. [27] demonstrated on the basis of thermal analysis and infrared

spectroscopy the conversion of hydroxyl groups to water, which becomes weakly and strongly hydrogen bonded to the kaolinite surface. This process is referred as the dehydroxylation of kaolinite where a) delamination of the crystal (due to grinding) exposes the inner surface hydroxyls to form water; and b) increased grinding results in the formation of an amorphous phase [21, 28, 29].

Simple sampling of infrared spectra may be carried out by the well known Diffuse Reflectance Fourier Transform Infrared (DRIFT) Spectroscopy method. However, the spectra can be quite broad and complex to interpret. Direct spectral comparison becomes difficult and curve fitting, which has been a popular method for infrared spectral resolution becomes problematic. A possible way to overcome this problem is to apply chemometrics techniques to extract information that is otherwise difficult to obtain from the complex raw spectra. In effect, chemometrics methods facilitate multivariate comparisons of spectra of samples, and there are numerous examples in the vibrational spectroscopy [30-33] and other literature [34-39] to attest the usefulness of this approach. However, the literature search did not reveal applications of chemometrics methods to the study of kaolinites and, in particular, to investigate the molecular and structural changes of different mechanochemically activated kaolinites.

This paper presents the results of an exploratory study of a set of DRIFT spectra of several different kaolinites with the aid of chemometrics. The assessment of DRIFT spectra was undertaken with the aid of Principal Components Analysis method (PCA), and the results were compared and contrasted with known information. In addition, an initial study on the application of the multi-criteria decision making methodology (MCDM), PROMETHEE (Preference Ranking Organisation METHod for Enrichment Evaluations) and GAIA (Geometrical Analysis for Interactive Assistance), was carried out to explore the relationships between spectroscopic data and other available information such as grinding time and chemical composition.

2 Experimental

2.1 Kaolinite samples

The samples used in the experiments were high grade natural kaolinites from four different sources: a) the Szegi (Hungary); b) the Kiralyhegy (Hungary); c) the Zettlitz (Carsbad, Czech Republic); and d) the Birdwood (South Australia). Their properties are shown in Table 1. The kaolinites were selected for their low quartz content and high purity (apart from the Kiralyhegy kaolinite). The analyses were undertaken by the authors and have been referred to in previous publications [26, 29].

2.2 Milling procedure

A Fritsch pulverisette 5/2-type laboratory planetary mill was used to grind the kaolinites. Samples were ground for 0, 1, 2, 3, 4, and/or 6 hours. Each milling was carried out with a 10 g air-dried sample in an 80 cm^3 capacity stainless steel (18 % Cr +8 % Ni) pot using 8 (31.6 g) stainless steel balls (10 mm diameter). The applied rotation speed was 374 r.p.m. All four kaolinite samples were ground under precisely the same conditions.

2.3 DRIFT spectroscopy

DRIFT spectra were sampled with the use of a Bio-Rad FTS 60A spectrometer (scans = 512; resolution = 2 cm^{-1}; mirror velocity = 0.3 cm/s).

Approximately 3 weight % of the kaolinite sample was dispersed in 100 mg oven dried spectroscopic grade KBr with a refractive index of 1.559 and a particle size of 5-20 μm. Reflected radiation was collected at ~50% efficiency. Background KBr spectra were obtained and spectra ratioed to the background. The DRIFT spectral accessory (Bio-Rad FTS) is a "praying mantis" design, and includes two four-position sample slides and eight sample cups. The cup (3 mm deep, 6 mm in diameter) accommodates powdery samples (1-3 % concentration) mixed with KBr, which were usually ground in an agate mortar and pestle. The reflectance spectra were expressed in Kubelka-Munk units, and are very similar to absorbance spectra.

2.4 DRIFT spectra

DRIFT spectra were baseline corrected, zero-offset and subdivided into three regions 400-830, 830-2030, 2600-3800 cm^{-1} (Spectracalc GRAMS). Thus, a data matrix for each spectral range consisted of 19 spectral objects and 250 wavenumber variables. Each matrix was then pretreated (Excel 5, Microsoft) prior to submission to PCA, and PROMETHEE and GAIA.

2.5 Chemometric analysis

2.5.1 Principal Component Analysis (PCA)

PCA is a well known chemometrics method [40, 41] facilitating pattern recognition and display of data. PCA effects multi-variate data reduction by transforming the data into orthogonal components, which are linear combinations of the original variables. These new variables are often referred to as latent variables or principal components (PCs). The transformation is achieved without loss of information because each PC accounts for a certain amount of data variance and the PCs are extracted in order such that PC1 accounts for largest amount of data variance, PC2 for the next largest amount and so on. The data reduction process often encapsulates all the significant information or data variance in just a few PCs instead of hundreds or even thousands of original variables (i.e. wavenumbers in the case of DRIFT spectra).

Each spectrum or object has a score value on each of the new PC variables and hence, PC score/score plots may be obtained e.g. a PC1 versus PC2 score plot may be displayed, which allows any patterns and trends to be studied. Commonly, such a score plot accounts for most of the data variance. In addition, each original variable (i.e. a wavenumber) is characterised by a loadings value, which expresses the importance of a variable on a particular PC for the discrimination of the objects (i.e. DRIFT spectra on a given PC). Hence, plots of loadings values for a given PC will indicate the wavenumber ranges that are principally responsible for the separation or discrimination of the objects or spectra on a given PC. However, it should be noted that loadings plots are generally regarded as abstract spectra and do not necessarily reflect a true spectral response from a particular component of sample mixture. Ultimately, a combination of the PC score/score plots and their corresponding

loadings displays may provide progressively more information which is often unavailable by conventional data analysis.

2.5.2 Data pretreatment

The raw data matrix consists of DRIFT spectra objects as rows with wavenumber variables as columns. To extract the data variance effectively, it is often necessary to rescale or pretreat the raw data matrix. In this work, the raw data matrix was double centred (i.e. y-mean scaled followed by x-mean scaling) [42]. This procedure removes the size component reflected by the first PC of the raw data matrix leaving essentially the information responsible for the data variance and noise. The resulting matrix was then submitted to variance scaling or standardisation to bring each column variable to unit variance. The pretreated matrix was then submitted to PCA.

2.5.3 PROMETHEE and GAIA

PROMETHEE and GAIA MCDM methods have been described in detail elsewhere [40, 43, 44]; in this paper, a summary of these methods is provided in sufficient detail to indicate the concepts and data treatment involved.

PROMETHEE is a non-parametric method used to rank a number of actions (objects) based on the criteria (variables) in the data matrix. For each criterion, a specific preference function, a threshold value and a weighting condition must be defined. The preference function is a mathematical function, which is used to calculate the degree of preference associated with each action. To set up a model for PROMETHEE, a preference function must be selected. In commercially available software (e.g. Decision Lab (Visual Decision 2000)), six shapes of preference functions are defined. In this software, they are called Usual, Linear, Level, V-shaped, U-shaped, and Gaussian [40]. For most functions, one or two classification thresholds must be provided by the user. These establish how preferences are to be attributed in accordance with the functions. *Minimised* and *maximised* conditions are allocated for each criterion to establish the preferred ranking sense. Therefore, the ranking can be undertaken bottom up (minimised) or top down (maximised) depending on the decision-maker's preferences. Weights can also be allocated for each criterion to reflect the importance of one criterion over another. By default, a weighting of 1 is assigned for all criteria. However, weights can be altered by the decision-maker if alternative scenarios are required in the investigation. The model is now set up according to the user's chosen scenario, and the raw data matrix may be submitted for calculation.

A summary of the PROMETHEE procedure is given below:

1. The raw data matrix is transformed into a difference *d* matrix.
2. For each criterion, the selected preference function, *P(a, b)* is applied to determine how much an outcome *a* is preferred to *b*. The overall outcome is a preference index matrix.
3. A global (or overall) preference index is then calculated for each object by summing all preference indices for each criterion.
4. Positive (Φ^+) and negative (Φ^-) outranking flows are calculated by summing all the global preference indices. Φ^+ describes how an action outranks all others while Φ^- describes how an action is outperformed by all others.

5. The outranking flows are compared pairwise according to a set of rules [40]. These are based on three possible outcomes, which lead to partial pre-order of the objects known as PROMETHEE I ranking:
    a) one action is preferred to another;
    b) there is no difference between the two actions; and
    c) the two actions can not be compared.
6. The net outranking flows ($\Phi = \Phi^+ - \Phi^-$) are calculated, which exclude rule 5 (c) above, and the results are displayed in a unidimensional (PROMETHEE II) ranking. Although it may be more convenient to use PROMETHEE II net ranking, some information does get lost in the process. This information is retained in the PROMETHEE I partial ranking, where incomparable objects (or alternatives) are displayed.

Typical partial PROMETHEE I and net PROMETHEE II rankings are illustrated in Figures 1a and 1b.

GAIA is a display method and is linked to the PROMETHEE procedure. The GAIA matrix is constructed from a decomposition of the Φ net outranking flows [40]. The data is then processed by a PCA algorithm, and displayed on a GAIA biplot, which shows a distribution of objects, criteria vectors and a decision axis, π. Such displays are interpreted conventionally as normal PCA biplots, and the decision axis π, displays the degree of decision power pointing to the approximate location of the preferred action. GAIA provides some guidance for criteria, which are important for net outranking, and which criteria influence the decision axis. An important difference between the application of the GAIA and a conventional PCA is its facility to model scenarios based on the choice of individual preference functions for each criterion, the choice of ranking sense and the criteria weights. The choice of such model specifications will be reflected in the distribution of the criteria vectors on the resulting biplot. This facilitates the testing of different experimental hypotheses, providing the user with options to test different scenarios. A typical simulated biplot is shown in Figure 1c.

3 Results and discussion

3.1 DRIFT spectra

The infrared spectra for the three regions are shown in Figures 2a, 2b and 2c. The first region (400-800 cm^{-1}) represents mainly the bands assigned to the OSiO and OAlO bending region. The second region (800-2030 cm^{-1}) mainly contains the SiO and AlO stretching modes and the third region (2600-3800 cm^{-1}) represents the OH stretching modes.

The three spectral regions show the effects of mechanochemical treatment of the kaolinite samples. The two regions of most interest are the first (OSiO and OAlO bending region) and the third (OH stretching region). In the first region, the spectra are complex and there is a significant overlap between the quartz and kaolinite bands (Figure 2a). The intense band at 780 cm^{-1} in the K series is attributed to quartz. Therefore, the Kiralyhegy (K) samples are clearly differentiated from the Birdwood (B), Zettlitz (Z) and Szegi (S) samples on the basis of its high quartz content. The spectral region 830 to 2030 cm^{-1} is shown in Figure 2b. This region is important as it shows the kaolinite SiO stretching vibrations.

The third region (OH stretching region, Figure 2c) is where most of the changes occur due to grinding (i.e. losing hydroxyl units, formation of water and

changes to the surface structure). According to Farmer [45], the hydroxyl stretching region of kaolinite displays five key features:

a) in-phase inner surface hydroxyl stretching vibration at 3695 cm^{-1};
b) two out-of-phase vibrations of the inner surface hydroxyl at 3668 and 3652 cm^{-1};
c) hydroxyl stretching vibration of the inner hydroxyl at 3620 cm^{-1};
d) transverse longitudinal optic vibration at 3684 cm^{-1}; and
e) water hydroxyl stretching vibration of weakly hydrogen-bonded interstitial water at 3595 cm^{-1}.

The DRIFT spectra of the four kaolinite samples exhibit these key features (Figure 2c). The two most significant spectral features are the reduction in peak intensities of the spectra with increase grinding time and the formation of the broad band in the 3000 – 3500 cm^{-1} range which is attributed to adsorbed and coordinated water [29]. This spectral region varies according to the kaolinite being studied. The intensity is significantly greater for the K3 and K 4 spectra compared with the S3, B3 and Z3 spectra (Figure 2c). The reason for this is that the presence of quartz in the Kiralyhegy kaolinite acts as an additional grinding medium which facilitates the formation of water. This water may be adsorbed or coordinated to the kaolinite surface.

Mechanochemical treatment results in dehydroxylation of the kaolinite. This occurs in two processes a) delamination of the kaolinite layers (exposing the hydroxyls to form water); and b) reaggregation of the crystallites to form a new amorphous material [12, 21, 28]. The effect of grinding is to reduce the layer stacking. Therefore, the effectiveness of mechanochemical treatment depends on the crystallinity of the kaolinite. For highly ordered kaolinites such as Kiralyhegy and Zettlitz, the effect of grinding can be quite significant. From Figure 2c, the formation of the water band at 3000-3500 cm^{-1} is clearly observed for the K and, to a lesser extent, the Z samples.

As discussed in the introduction, the ground kaolinite particles agglomerate to take on a spherical shape. This means that during the grinding process, the particles recombine to form spheres. Gonzalez Garcia [27] suggests that grinding causes the particles to fragment and form stable large spheroidal aggregates of fine particles. The effectiveness of the mechnomechemical treatment was found to be dependent on the formation of these spheres, particle size and the crystallinity of the original kaolinite sample.

Generally, the spectra display significant changes in some regions and less in others. Therefore, it is difficult to compare the spectra for the four samples and study the effects of grinding comprehensively. To facilitate this work, chemometric techniques (PCA, and PROMETHEE and GAIA) were used to investigate and classify the samples, and assist with the interpretation of results.

3.2 Chemometrics

3.2.1 PCA

PC1 versus PC2 scores plots for the three spectral regions are shown in Figures 3, 4 and 5. Each pair of PCs accounts for at least 80% of the data variance (i.e. most of the differences in the spectra).

In the 400-800 cm^{-1}region (Figure 3a), it can be seen that the spectra of the kaolinite samples have been separated into two groups: K (negative scores on PC1); and B, Z and S (positive scores on PC1). The K series samples have a high quartz content and the loadings plot for PC1 indicates that the separation of the K series spectra occurs on the basis of frequency ranges attributable to quartz vibrations

(Figure 3b). It is evident that the K series objects are spread out along PC1 but are not ranked according to grinding time on this PC; in contrast, the objects from the Z, B, and S series cluster fairly closely in two groups with the Z group closer to the origin followed by objects from the B and S series with more positive PC scores. A general conclusion from these observations is that the Z, B and S series show less effect on mechanochemical grinding as reflected by the DRIFT criterion in this spectral region.

PC2 shows that the K objects are nearly rank ordered according to grinding time with K0 having the most positive score and K4 the most negative score. Only K1 is displaced from the series on PC2. The Z objects cluster (with positive scores) is separated on the basis of spectral changes in the kaolinite bands at 474 cm^{-1} and 540 cm^{-1} (Figure 3c). Objects with negative scores on PC2 are separated on the basis of spectral changes around the quartz bands at 512 cm^{-1}, kaolinite bands at 644 and 622 cm^{-1}, and mixtures of quartz and kaolinite vibrations at ca 700 and 800 cm^{-1}. Again there is no rank order with grinding in Z, B or S series.

In the 830-2030 cm^{-1} region (Figure 4a), the spectra of the K series form a cluster with negative scores on PC1 and are clearly separated on the basis of the 900-1250 cm^{-1} range which accommodates typical bands of quartz and kaolinite. Since the loading intensities are relatively high, the discrimination of this series from the B and S objects is on the basis of changes to the stretching vibrational modes of both kaolinite and quartz (i.e. deformation of both the lattices). The Z series of objects, which is located principally around the origin, does not contribute much to PC1. This emphasises once again its difference not only from the K series but also from the B and S series.

In addition, the grinding time does not appear to have a significant affect on the score plots of the B, Z and S series. These samples form relatively compact groups as they did in Figure 3a on the positive PC1 axis. It is worth noting that there is also a high correlation between the B and S series, possibly due to similar structural disorder. In general, there appears to be no order due to grinding time for this region.

In the 2600-3800 cm^{-1} region (Figure 5a), the PC1 versus PC2 scores plot shows some apparent correlation with respect to grinding time. Both the K and Z samples are highly ordered on the PC1 axis in order of grinding time. The objects positive on PC1 are discriminated by a broad band of positive loadings in the 3000-3570 cm^{-1} range. This is attributed to OH stretching vibrations principally of weakly H-bonded water (nominally at 3550 cm^{-1}). The spectral objects with negative PC1 scores are discriminated on the basis of a broad loadings band in the 2600-3000cm^{-1} that is attributed to OH stretching vibrations principally those of strongly H-bonded water. The negative loadings at around 3750 cm^{-1} have no specific spectral association. Thus, it appears that the ranking of the K and the Z series is associated with changes in the inner surface and inner OH groups of the kaolinite and the formation of water during grinding (i.e. dehydroxylation of kaolinite).

In contrast, B and S spectral objects are less affected by the dehydroxylation process (due to grinding) on PC1 and remain more or less randomly associated with OH stretching vibrations. This suggests that the grinding process is affecting these kaolinite samples differently. On PC2, the S and B spectra (positive PC2 scores) are associated with the high loadings centred on ca. 3000 cm^{-1}. In accordance with band assignments by Farmer [45], this band of loadings is attributed principally to OH stretching vibrations of strongly H-bonded water. Thus, the discrimination of the S and the B series of spectra on PC1 and PC2 are consistent.

Apparent ordering with respect to grinding time was observed for both K and Z spectral objects but not for B and S spectral objects. This may be due to the structural disorder of B and S samples, specifically:

a) B samples are complex and include a highly disordered kaolinite film coating the highly ordered kaolinite crystals [47]. Previous studies have shown that the kaolinite from Birdwood, South Australia is a highly ordered kaolinite with a very high Hinckley Index [47, 48]. TEM images show the presence of two types of kaolinite a highly ordered kaolinite coated by a disordered kaolinite. This disordered kaolinite coating may prevent the dehydroxylation process observed in K and Z samples. Previous studies have also shown the kaolinite is difficult to intercalate [46, 47, 49, 50].
b) S samples are naturally highly disordered and, thus, grinding has a minimum effect. This is in contrast to K and Z samples, which are highly ordered and undergo significant changes in the hydroxyl region with grinding especially since quartz is present naturally.

There is a clear discrimination of the spectral objects with negative PC2 scores on the basis of changes in the kaolinite OH vibrations given the high negative loadings in the 3500-3700cm^{-1}. Again, the K series objects are well ordered according to their grinding time and the Z series spectra are roughly ordered. This observation suggests that the presence of natural quartz is of considerable significance to the grinding of the K series, and probably to kaolinites in general (i.e. quartz enhances the delamination process). The ordering of quartz according to the SiO deformation band at ca 512cm^{-1} as discussed for the 400-830cm^{-1} region suggests that quartz itself changes during initial time of grinding. This is in agreement with the work of Schrader [51] which showed that for grinding of quartz important changes occur in the first few hours. In addition, the rank ordering of the K spectral objects on PC2 on the basis of the 3500-3700cm^{-1} loadings indicates that the kaolinite OH are being affected in parallel with the quartz.

It has been noted in the above discussion that kaolinite forms small spheres during grinding whereas the samples with large amounts of natural quartz would tend to disperse the kaolinite. The grinding between kaolinite spheres would occur only at their points of contact, which for a given particle are unlikely to be more than six at any instant. The dispersed kaolinite will be ground not only by larger areas of contact between kaolinite particles but also by contact with the quartz crystals. Thus, it is suggested that the presence of the dispersed kaolinite sample as well as that of natural quartz lead to a different and mechanically much more efficient grinding process. This is reflected in a greater relationship between grinding time and K spectral objects, where the presence of natural quartz has enhanced the grinding process.

3.2.2 PROMETHEE and GAIA

The above PCA treats only the spectral data and it is difficult to study any comparisons and influence of other variables of interest such as the composition of the samples and any physical properties such as grinding time on the spectra. In the case of the latter, one could infer from the PC scores (Figure 5a) that the grinding time played an important role in the distribution of the K and Z objects in the PC plane. However, it may be possible to obtain more definitive information by submitting the spectral data in a different format and in differently constructed matrices to PROMETHEE and GAIA for analysis.

As previously indicated with PROMETHEE, it is necessary to model each criterion independently. This makes it possible to have very different criteria e.g. chemical composition variables, physical attributes, biological characteristics, sociological traits etc to be compared in the same matrix. Spectral data could be introduced into such a matrix if the spectral information could be represented in

compressed form by new variables without loss of spectral information. This is precisely what PCA performs – the new variables being the PCs, and theoretically all spectral information is contained in the several significant PCs without loss of information. It follows that PCs may be used as criteria to represent spectra in a PROMETHEE matrix with scores being the new data. The application of this approach is illustrated in one of the investigated scenarios below. However, it should be recalled that the PC scores commonly have positive and negative values, whereas PROMETHEE cannot account for both positive and negative values with some of the preference functions e.g. the commonly used Linear V-shaped model, which is bounded by zero and either a positive or a negative *p* threshold. In such cases, there are three possible alternatives: a) select a preference function which recognises the '-' / '+' sign difference, e.g. the Usual function which only has two preference values , either 0 or 1 – this approach is often unsatisfactory for the distribution of criterion values; b) the negative score values are left in their raw state – in which case for the commonly used linear V-shaped preference function with a *maximised* criterion, such scores will have a zero preference value, which could bias the analysis; and c) the baseline for the scores could be shifted by adding to each score the absolute value of the lowest negative score. In the present study, both operations b) and c) have been performed, and it was found little or no influence in either the ranking or the GAIA biplot display after changing the baseline as described.

One of the advantages of PROMETHEE is that it is a non-parametric method, which means that in principle it is possible to compare as few as two objects. Thus, the investigation was undertaken on a small data matrix consisting of the four original unground samples of kaolinites as objects for which physical ((i.e. Hinckley index (HI) and loss on ignition (LOI)) and chemical (elemental composition) data are available as well as the IR spectra.

Therefore, the 4 x 5 matrix consisted of four unground kaolinite objects and five criteria including the major chemical variables of kaolinite (silicate (SiO_2), alumina (Al_2O_3) and natural quartz) as well as physical properties (HI and LOI) (Table 2). The Linear V- shaped preference function was applied for all five criteria, and all of the five variables except LOI were set to maximise. This setting indicates that high values for the four variables are preferred while for LOI low values dominate. The weights for each of the five variables were set to 1.

The model parameters described above imply that in the GAIA biplot, the quartz and silica loading vectors should point roughly in the direction of the K object and both should be quite strong as this object clearly has the highest values for these criteria; the same object has by far the lowest value of LOI and this vector should cluster with the other two as well. The alumina vector should point roughly to the B object, which is high in alumina, and the HI index (being an index of crystallinity) should be essentially independent of the elemental composition. It therefore, should be approximately at right angles to the other loadings vectors.

The data matrix discussed above was submitted to PROMETHEE and GAIA with results presented in Figure 6.

The GAIA biplot (Figure 6, 99.5% variance described) is consistent with the description provided in the scenario above with the silicate (SiO_2), quartz and LOI criteria vectors grouping together, and pointing roughly towards the K object, which has high PC1 scores. On the other hand, the alumina (Al_2O_3) vector points roughly towards the B object as anticipated, and importantly the HI vector is approximately at right angles to the other vectors. Such agreement between the scenario interpretation by the model and the analysis strongly suggests that sensible results may be obtained from such MCDM analysis. This also indicates that similar analysis carried out on

matrices where scenarios are more difficult to propose will nevertheless provide useful information.

The PROMETHEE II net outflow rank order is K0 (Φ= 0.35) >B0 (Φ= -0.04) >Z0 (Φ= -0.10) >S0 (Φ= -0.21) with the four net outflow indices, Φ, well separated from each other. Interestingly, the B0 object is ranked second on the basis of the model. According to the GAIA plot, this is presumably because of its high kaolinite content being dominated only by silica/quartz rich K0 sample.

When the dominance of the K0 sample, because of its very high quartz content is removed by excluding this object and the data matrix is re-analysed without any changes to the model, the resulting biplot (Figure 7, 100% variance described) shows certain important similarities with the previous biplot (Figure 6). Thus, vectors SiO_2, LOI and quartz still group together and point to the object, Z0, which is relatively rich on the SiO_2 and quartz criteria, and the loading vector, HI, is independent of the other three. But now, it is the physical variables that dominate the biplot.

For the third MCDM experiment, all model parameters for the five criteria remain the same but minor chemical components were added (MgO, CaO, Fe_2O_3, Na_2O, K_2O, TiO_2), as well as PC1 and PC2 scores taken from the PCA of the spectra for the 400-830 cm^{-1} region (Table 3). The same linear preference functions were used and these new criteria were set to maximise.

From the model described above, the major chemical components (SiO_2, Al_2O_3 and quartz) and physical parameters should behave in a similar manner as described in the previous model (Figure 6). Therefore, SiO_2, quartz and LOI should cluster close together and point roughly in the direction of K0. Al_2O_3 should point roughly in the direction of B0 (with its kaolinite rich samples) and HI should be perpendicular to the other criteria. With the addition of the minor chemical components, it is anticipated that these criteria would cluster together and point towards the kaolinite rich samples (i.e. Al_2O_3) rather than SiO_2 and quartz. The minor chemical components relate to the presence of impurities such as feldspar, iron oxides, illite and goethite in the kaolinite samples. The common feldspars can include sodium (Na), potassium (K), and/or calcium (Ca) in its composition. Goethite is a common iron mineral. The other key impurity in the kaolinite samples is K containing illite. Illite is a common clay mineral found in soils.

However, it should be noted that the physical parameters may also influence the position of the minor chemical components, especially HI which accounts for crystallinity of the kaolinite samples. PC1 should discriminate quartz rich samples from kaolinite rich samples as well as the degree of crystallinity of the kaolinites. Positive PC1 therefore, describes quartz rich, highly crystalline samples and negative PC1 describes kaolinite rich, low crystalline samples. Thus, PC1 should point towards either the kaolinite rich or quartz rich spectral objects. And PC2 should be aligned perpendicular to the PC1 vector.

The GAIA biplot (Figure 8, 87.8% variance described) is consistent with the above scenario described. SiO_2, quartz and LOI criteria vectors are clustered together and point towards K0 while Al_2O_3 point towards the kaolinite rich samples. HI is roughly perpendicular to the major chemical component vectors and LOI, and point towards K0 and B0 (i.e. high crystalline kaolinite samples). The minor chemical components are clustered together with the exception of K_2O which is aligned closely with Al_2O_3 vector. The GAIA biplot also indicates that S0 and, to a lesser extent, Z0 are different from the other two samples (K0 and B0) due to the minor chemical components. Since all these variables (MgO, Na_2O, Fe_2O_3, CaO) are correlated with S0, it can be concluded that feldspar is significant in S0 (Table 1). Similarly, Al_2O_3 and K_2O vectors are closely correlated therefore, it can also be concluded that Z0 contains illite as impurities (Table 1). Thus, the minor chemical composition

variables have provided additional information regarding the samples that were not available in the previous PROMETHEE model.

With respect to PC variables, it is apparent that PC1 is separating the samples on the basis of the quartz/kaolinite contribution. PC1 is closely related to the Al_2O_3 criteria and pointed in direction of the kaolinite rich samples. This finding supports the conclusion from the PCA.

The PROMETHEE II net ranking, S0 (Φ= 0.08) >K0 (Φ= -0.03) >Z0 (Φ= -0.01) >B0 (Φ= -0.09), for this analysis illustrates that minor chemical composition influences the ranking process, and the Φ net ranking range has been substantially compressed by a factor of about three. This suggests that the discrimination of the samples is substantially reduced. From the GAIA biplot (Figure 8), the decision axis (π) is closely correlated with the MgO vector, and to a lesser extent with Na_2O, Fe_2O_3, and CaO vectors. It appears that the level of impurities in the kaolinite samples is determining the rank order. For example, S0 contains feldspar, K0 contains high proportion of natural quartz and Z0 contains illite. What the PROMETHEE and GAIA analysis suggests is that B0 is the most pure kaolinite sample out of the four kaolinites used in this study.

An attempt has been made to explore other relationships with the use of the above novel application of PROMETHEE and GAIA. This application can be extended to further investigate the apparent observation from the PCA for the OH region (i.e. grinding time was correlated with the K and Z spectral objects) (Figure 5a). In the PCA context, it was not possible to introduce the grinding time variable amongst the spectral frequencies. However, as indicated above, the spectra can be modelled with the use of PC scores in the PROMETHEE matrix.

Thus, for the fourth MCDM experiment, a model was constructed to explore a relationship between grinding time and the kaolinite spectral objects. The 19 x 3 matrix consisted of nineteen kaolinite objects and three criteria including PC1 scores, PC2 scores and grinding time loadings (Table 4). The V-shaped linear function was applied for all three criteria and PCs were set to maximise while grinding time was set to minimise. This setting indicates that high values are preferred for PCs and low values are preferred for grinding time. The weights for each of the three criteria were set to 1.

From the model described above, the spectral objects should align ideally with the grinding time vector in the GAIA biplot, if there is a close correlation between the spectral objects and the grinding time loadings variable. However, since the kaolinite samples are inherently different, other physico-chemical properties as reflected by the spectral variables may interfere to shift the objects roughly in parallel with the grinding time vector. Note this could occur only if the interference effects are relatively minor and grinding is still the dominant variable.

A matrix of spectral objects (K, S, Z and B), spectral PCs scores and grinding time loadings variables were submitted to PROMETHEE for analysis (Table 4) and the results presented in Figure 9.

The GAIA biplot (Figure 9, 92.6% variance described) displays the relationships between the spectral objects, spectral PC variables and grinding time vector. From Figure 9, K and Z spectral objects are roughly parallel with the grinding time vector, and it is the only criterion vector with which the K and the Z series have any systematic association. This supports the initial PCA observation regarding an apparent trend between grinding time and the K and Z kaolinite samples as reflected by their DRIFT spectra. In contrast, the B and S spectral objects are clustered together and there is no observed relationship with grinding time (although arguably there is some non-systematic association with PC2) for these spectral objects.

4 Conclusions

In general, this study demonstrated that DRIFT spectra of different kaolinites can be successfully compared and interpreted in respect to their grinding by the common chemometrics display method, PCA. In addition, it was shown how the kaolinites may be globally compared on the basis of their chemical composition and physical properties, and how their spectral characteristics may be included in such comparisons with the aid of the MCDM methods, PROMETHEE and GAIA.

The band assignments of the DRIFT spectra of mechanochemically ground kaolinite samples originating from Kiralhegy (Hungary), Szegi (Hungary), Zettlitz (Slovakia) and Birdwood (Australia), were generally consistent with those found in the literature. The three spectral regions chosen for interpretation viz,. 400-800, 800-2030, 2600-3800 cm^{-1}, were then analysed by the two different chemometrics approaches.

In regard to PCA, for each of the spectral regions, a PC scores plot was analysed in some detail with the aid of loadings plots. The scores plots produced concise displays of all the spectral data and allowed a comparative examination of the spectra. In general, the clustering could be interpreted in terms of the known properties of kaolinite samples as well as the presence of natural quartz. The dominance of this component was a notable feature in the two PC scores plots for the first two spectral regions by the distinctive discrimination of the Kiralhegy spectral objects. In addition, the close intermixing of the Birdwood and Szeg series spectral objects was quite apparent, and since these two samples are from completely different geographical regions, it is clear that this variable is not reflected in the DRIFT spectra. Importantly, while some ordering of the objects in some PC clusters was apparent, it was not according to the grinding time sequence. Thus, it would appear that neither the kaolinite nor the quartz, are systematically responsive to grinding time according to the spectral criteria.

The third spectral region, attributed to the OH vibrations, was the only one to show apparent systematic ordering of the Kiralhegy and, to a lesser extent, Zettlitz spectral objects with grinding time. These two series of objects displayed roughly linear trends in the PC spectral plane. This was attributed to the effect of the natural quartz on the delamination of kaolinite and the accompanying phenomena such as the formation of kaolinite spheres and water.

With the MCDM methods, it was firstly shown that sensible inter-relationships between physical and major chemical criteria were reflected by the net outranking flows and GAIA biplot displays. Then, it was demonstrated that minor chemical components can influence the rank order of the objects as well as indicating that the Birdwood sample is arguably the most pure kaolinite sample analysed. And finally, some support for the apparent trend with grinding time as noted in the PC plot of the OH spectral region, was obtained from the last MCDM experiment. The key observation was that the Kiralhegy and Zettlitz objects formed roughly linear trends in parallel with the grinding time criterion vector.

References

1. H. H. Murray, W.M. Bundy, C.C. Harvey (Eds), The Clay Miner Soc. (1993) 1.
2. P. A. Ciullo, Industrial Minerals and Their Uses: A Handbook and Formulary (1996).
3. T. Kendall, Industrial Clays: An Industrial Minerals Special Review (1996).
4. R.L. Frost, J. Kristof, G.N. Paroz, J.T. Kloprogge, J. Colloid and Interface Sci. 208 (1998) 478-486.
5. R. L. Frost, J. Kristof, E. Horvath, J.T. Kloprogge, Langmuir 16 (2000) 5403.
6. D.R. Collins, C.R.A. Catlow, Acta Crystallogr. B47 (1991) 678.
7. H. Takahashi, Clays, Clay Minerals. Proc. Natl. Conf. Clays, Clay Minerals, 6th, Berkeley (1959) 279.
8. H. Takahashi, Bull. Chem. Soc. Japan 32 (1959) 235.
9. H. Takahashi, Bull. Chem. Soc. Japan 32 (1959) 245.
10. H. Takahashi, Bull. Chem. Soc. Japan 32 (1959) 252.
11. J. Wiegmann, G. Kranz, Silikat. Tech. 8 (1957) 520.
12. Z. Juhasz, Acta Mineral.-Petrogr. 24 (1980) 121.
13. Z. Juhasz, I. Wojnarovits, CFI, Ceram. Forum Int. 61 (1984) 131.
14. W. D. Laws, J. B. Page, Soil Sci. 62 (1946) 319.
15. R. Schrader, Silikat. Tech. 21 (1970) 196.
16. E. Kohler, Y. Hofmann, E Scharrer, K. Fruhauf, Ber. der Deutsch. Deram. Ges. 37 (1960) 493.
17. S. J. Gregg, K. F. Hill, T. V. Parker, J. App. Chem. 4 (1945) 666.
18. J. Sanyal, D. Lahiri, Trans Ind. Ceram. Soc. 20 (1961) 11.
19. G. R. Blair, A.C.D. Chaklader, J. Thermal. Anal.4 (1971) 311.
20. T. Haase, K. Winter, Bull. Soc. Franc. Ceram. 44 (1959) 13.
21. F. Gonzalez Garcia, M. T. Ruiz Abrio, M. Gonzalez Rodriguez, Clays Clay Miner. 26 (1991) 549.
22. S. Yariv, Clays Clay Miner. 23 (1975) 80.
23. V. C. Farmer, Clays Clay Miner. 33 (1998) 601.
24. J. G. Miller, T. D. Oulton, Clays Clay Miner. 18 (1970) 313.
25. R. L. Frost, J. Kristof, E. Horvath, J.T. Kloprogge, Langmuir 15 (1999) 8787.
26. R. L. Frost, J. Kristof, E. Horvath, J.T. Kloprogge, Langmuir 17 (2001) 3216.
27. F. Gonzalez Garcia, M. Gonzalez Rodriguez, C. Gonzalez Vilchez, M. Raigon Pichardo, Bol. Soc. Esp. Ceram. Vidrio. 31 (1992) 297.
28. E. F. Aglietti, J. M. Porto Lopez, E. Pereira, J. Min Proc. 16 (1986) 135.
29. R. L. Frost, J. Kristof, E. Mako, W. N. Martens, Langmuir 18 (2002) 6491.
30. M. Andersson, K. Knuuttila, Vib. Spec. 29 (2002) 133.
31. S. B. Engelsen, L. Norgaards, Carbohydrate Polymers 30 (1996) 9.
32. J. Jiang, Y. Ozaki, App. Spec. Rev. 37 (2002) 321.
33. H. Schulz, B. Schrader, R. Quilitzsch, S. Pfeffer, H. Krueger, J. Agric. Food. Chem. 51 (2003) 2475.
34. C. Armanino., M. R. Festa, Analytica Chimica Acta, 331 (1996) 43.
35. H. L. MacDonald, H. Liu, P. Yager, Biomed. Fiber Optic Instr. 2131 (1994) 514.
36. L. Campanella, G. De Angelis, G. Visco, Anal. Bioanal. Chem. 376 (2003) 467.
37. L. F. Capitan-vallvey, R. Avidad, M. D. Fernandez-Ramos, A. Ariza-Avidad, E. Arroyo, Anal. Bioanal. Chem. 373 (2002) 289.
38. K. Florian, M. Matherny, N. Pliesovsha, Microchemical J. 51 (1995) 26.
39. E. M. Rodriguez Rodriguez, M. Sanz Alaejos, C. Diaz Romero, J. Agric. Food Chem. 47 (1999) 1520.
40. H. R. Keller, D. L. Massart, J. P. Brans, Chemometrics Intelligent Lab. Sys. 11 (1991) 175.

41. N. J. Martin, B. St Onge, J. Waaub, J. Env. Pollution 12 (1999) 264.
42. S. Kokot, G. King, H. R. Keller, D. L. Massart, Analytica Chimica Acta 268 (1992) 81.
43. J. P. Brans and P. Vincke, Mangt Sci. 31 (1985) 647.
44. J. P. Brans, B. Mareschal, P. Vincke, EJOR, 24 (1986) 228.
45. V.C. Farmer, Mineral Society Monograph 4: The Infrared Spectra of Minerals, Mineral Society, London, 1974.
46. Frost, R. L., Horvath, E., Mako, E., Kristof, J. and Redey, A., *Thermochim. Acta* 408**,** (2003) 103.
47. Frost, R. L., Van Der Gaast, S. J., Zbik, M., Kloprogge, J. T. and Paroz, G. N., *Appl. Clay Sci.* 20**,** (2002) 177.
48. Paroz, G. N., Frost, R. L. and Cash, G. A., *AIP Conf. Proc.* 430**,** (1998) 678.
49. Frost, R. L., Kristof, J., Ding, Z. and Horvath, E., *2001 a Clay Odyssey, Proceedings of the International Clay Conference, 12th, Bahia Blanca, Argentina, July 22-28, 2001* (2003) 523.
50. Kristof, J., Horvath, E., Frost, R. L. and Kloprogge, J. T., *J. Therm. Anal. Calorim.* 63**,** (2001) 279.
51. R. Schrader, Kristall und Technik, 1 (1966) 59-75.

List of Tables

Table 1.

	Kiralyhegy (K) wt%	Szegi (S) wt%	Zettlitz (Z) wt%	Birdwood (B) wt%
SiO_2	81.59	46.89	46.97	46.97
Al_2O_3	12.10	33.51	36.32	38.12
Fe_2O_3	0.07	3.1	0.37	0.17
CaO	0.35	0.53	0.54	0.14
MgO	0.51	0.71	0.26	0.07
K_2O	0.05	0.35	1.21	0.21
Na_2O	0.03	0.16	-	-
TiO_2	-	0.06	0.05	0.01
Loss on Ignition (LOI)	5.1	14.3	12.9	15.3
Kaolinite	67	95	92	99
Quartz	33	2	4	0.5
Illite	-	-	4	-
Feldspar	-	3	-	-
Hinckley Index (HI)	1.4	0.4	0.7	1.3

Table 2.

Kaolinite sample	SiO_2 (wt%)	Al_2O_3 (wt%)	Quartz (wt%)	HI	LOI (%)
K0	81.6	12.1	67.0	1.4	5.1
S0	46.9	33.5	2.0	0.4	14.3
Z0	47.0	36.3	4.0	0.7	12.9
B0	47.0	38.1	0.5	1.3	15.3

Table 3.

Kaolinite sample	MgO (wt%)	CaO (wt%)	Fe_2O_3 (wt%)	K_2O (wt%)	NaO_2 (wt%)	TiO_2 (wt%)	PC1 scores	PC2 scores
K0	0.5	0.4	0.1	0.1	-	-	8.4	-2.0
S0	0.7	0.5	3.1	0.4	0.2	0.1	3.1	17.5
Z0	0.3	0.5	0.4	1.2	-	0.1	-13.1	7.2
B0	0.1	0.1	0.2	0.2	-	-	1.3	6.6

Table 4.

Kaolinite sample	PC1 scores	PC2 scores	Grinding time (h)
K0	-13.1	7.2	0
K1	-17.3	-3.2	1
K2	-26.3	0.9	2
K3	-23.0	-4.8	3
K4	-12.1	-13.3	4
S0	8.4	-2.0	0
S1	10.7	-9.0	1
S2	10.4	-8.1	2
S3	7.4	-0.2	3
S6	10.0	-6.0	6
Z0	1.3	6.6	0
Z1	2.9	6.0	1
Z2	3.0	7.6	2
Z3	4.6	4.1	3
Z4	4.1	4.8	4
B0	3.1	17.5	0
B1	7.9	-0.8	1
B2	7.7	0.6	2
B3	10.7	-7.9	3

List of Figures

Figure 1.

(a)

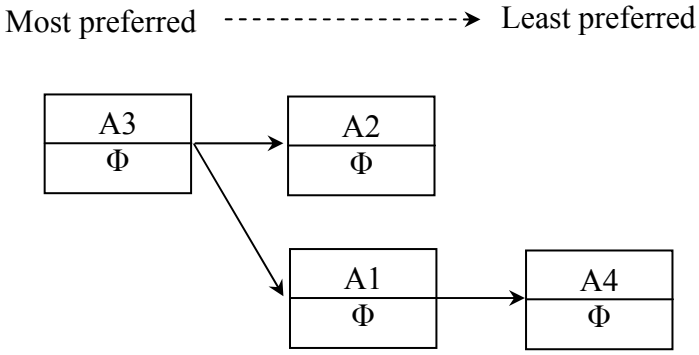
Most preferred
Least preferred
A3
Φ
A2
Φ
A1
Φ
A4
Φ

(b)

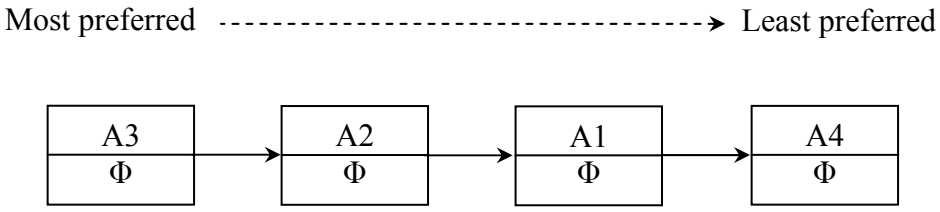
Most preferred
Least preferred
A3
Φ
A2
Φ
A1
Φ
A4
Φ

(c)

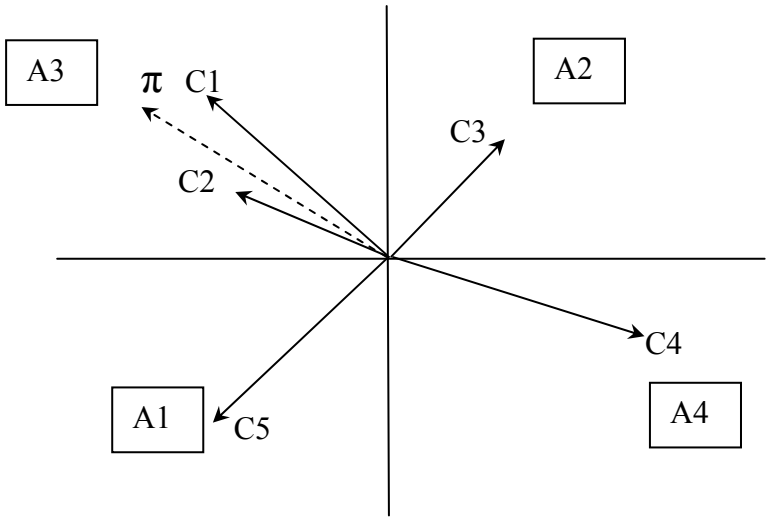
A3
π
C1
A2
C3
C2
C4
A1
C5
A4

Figure 2

(a)

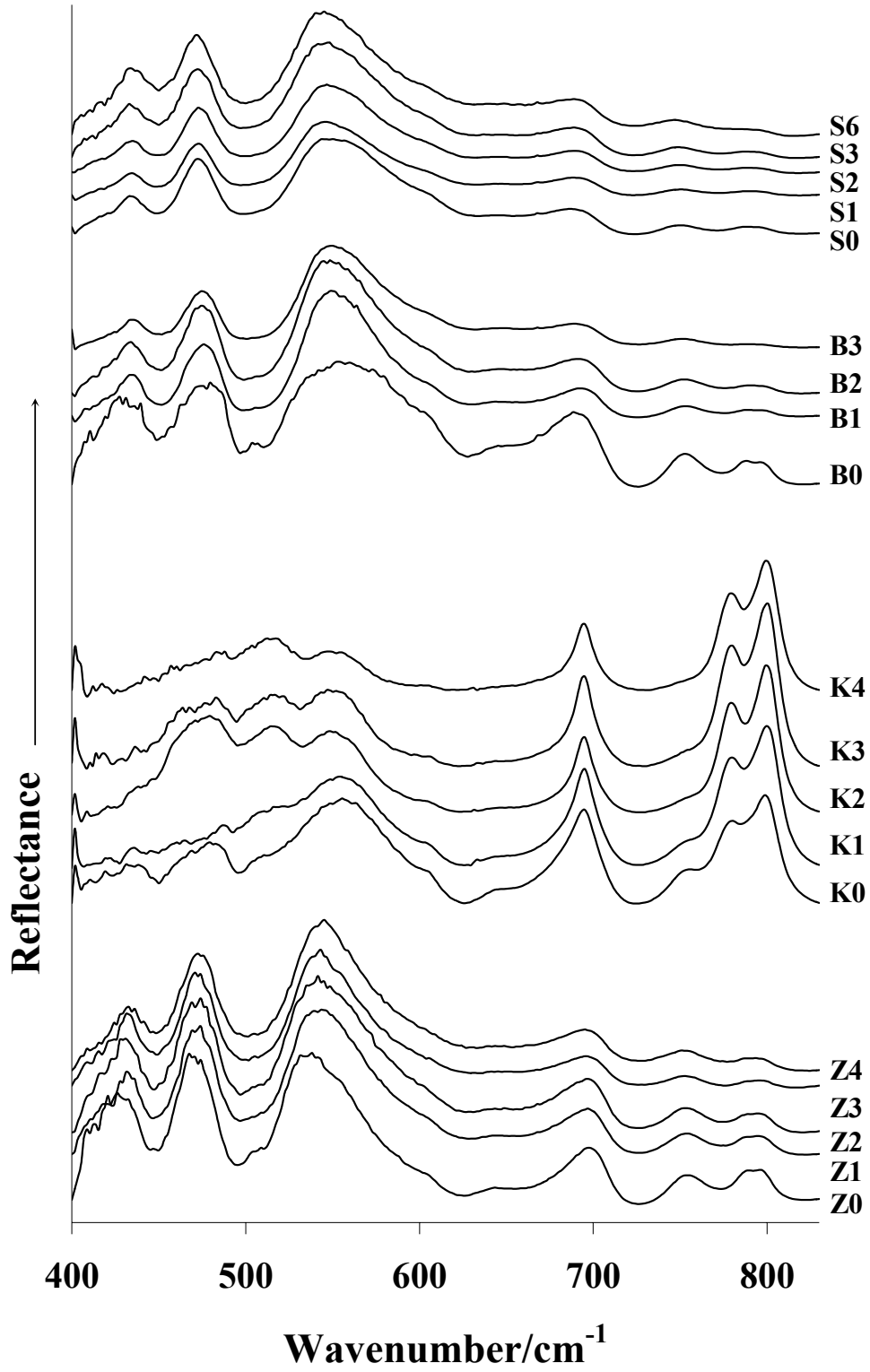
S6
S3
S2
S1
S0
B3
B2
B1
B0
K4
K3
K2
K1
K0
Z4
Z3
Z2
Z1
Z0
Reflectance
400
500
600
700
800
Wavenumber/cm-1

(b)

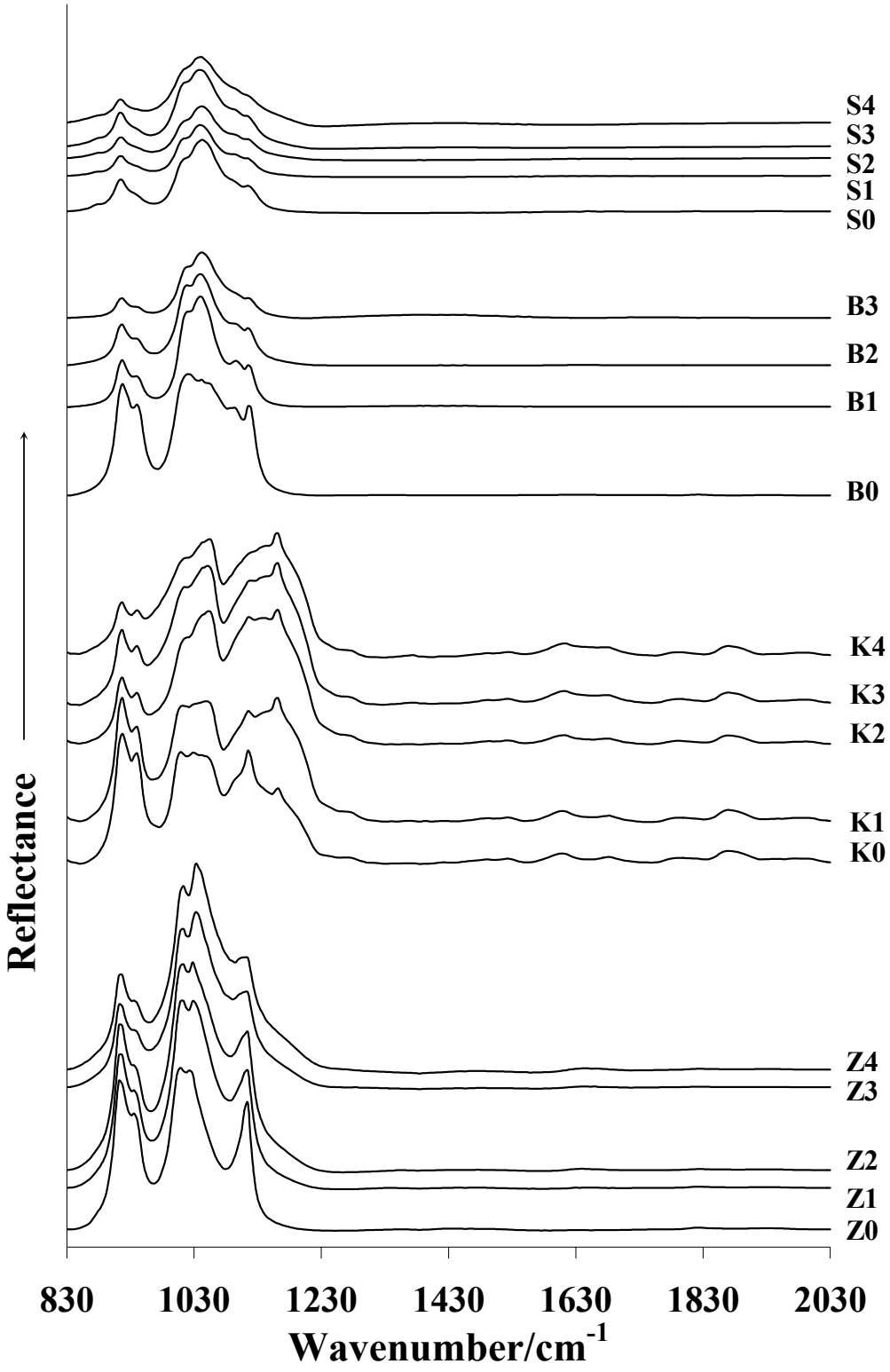
S4
S3
S2
S1
S0
B3
B2
B1
B0
K4
K3
K2
K1
K0
Z4
Z3
Z2
Z1
Z0
Reflectance
830
1030
1230
1430
1630
1830
2030
Wavenumber/cm-1

(c)

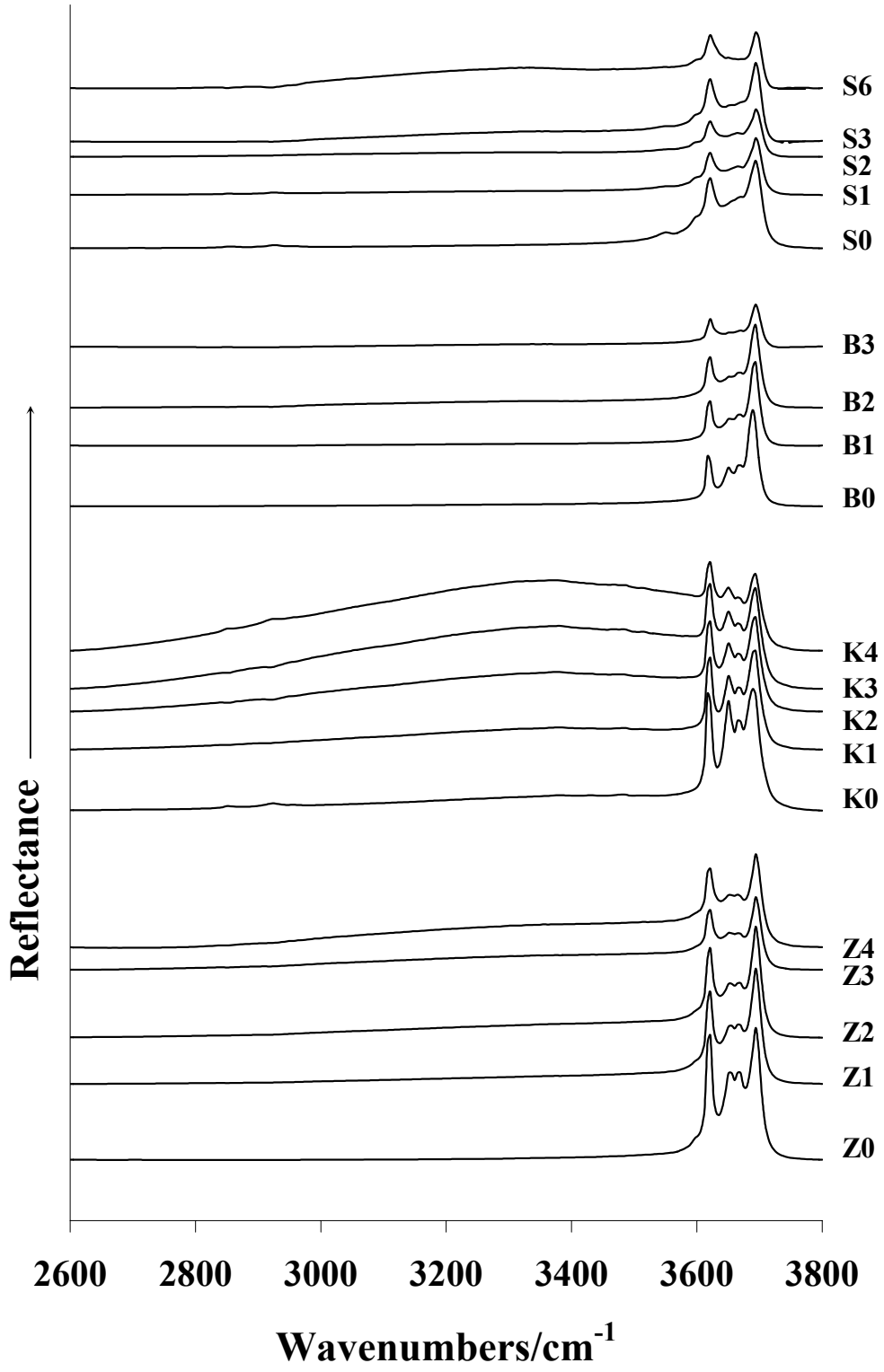
S6
S3
S2
S1
S0
B3
B2
B1
B0
K4
K3
K2
K1
K0
Z4
Z3
Z2
Z1
Z0
Reflectance
2600
2800
3000
3200
3400
3600
3800
Wavenumbers/cm-1

Figure 3.

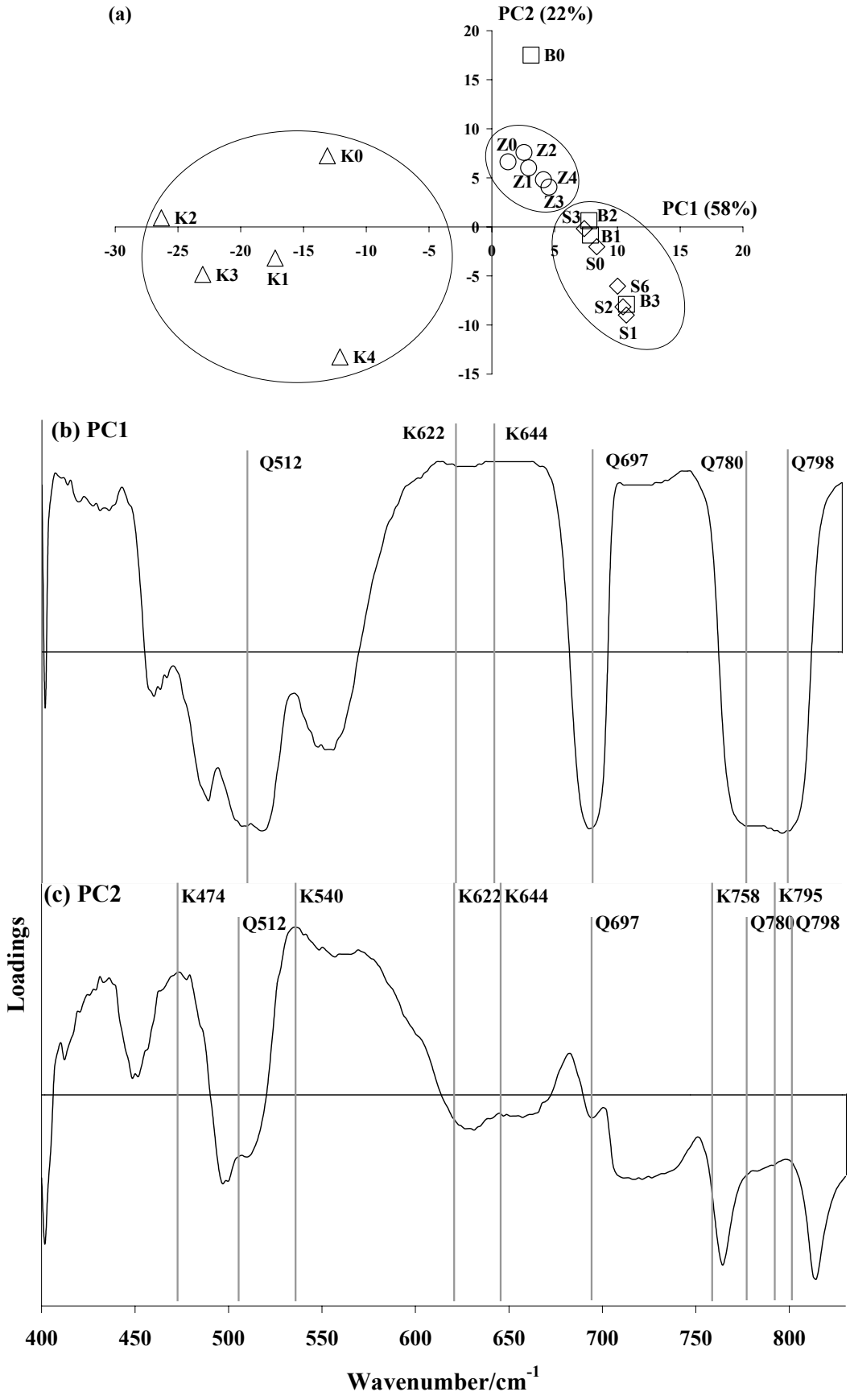
(a)
PC2 (22%)
PC1 (58%)
B0
Z0
Z2
Z1
Z4
Z3
S3
B2
B1
S0
S6
B3
S2
S1
K0
K2
K3
K1
K4
(b) PC1
Q512
K622
K644
Q697
Q780
Q798
(c) PC2
K474
K540
K622
K644
K758
K795
Q512
Q697
Q780
Q798
Loadings
Wavenumber/cm-1

Figure 4.

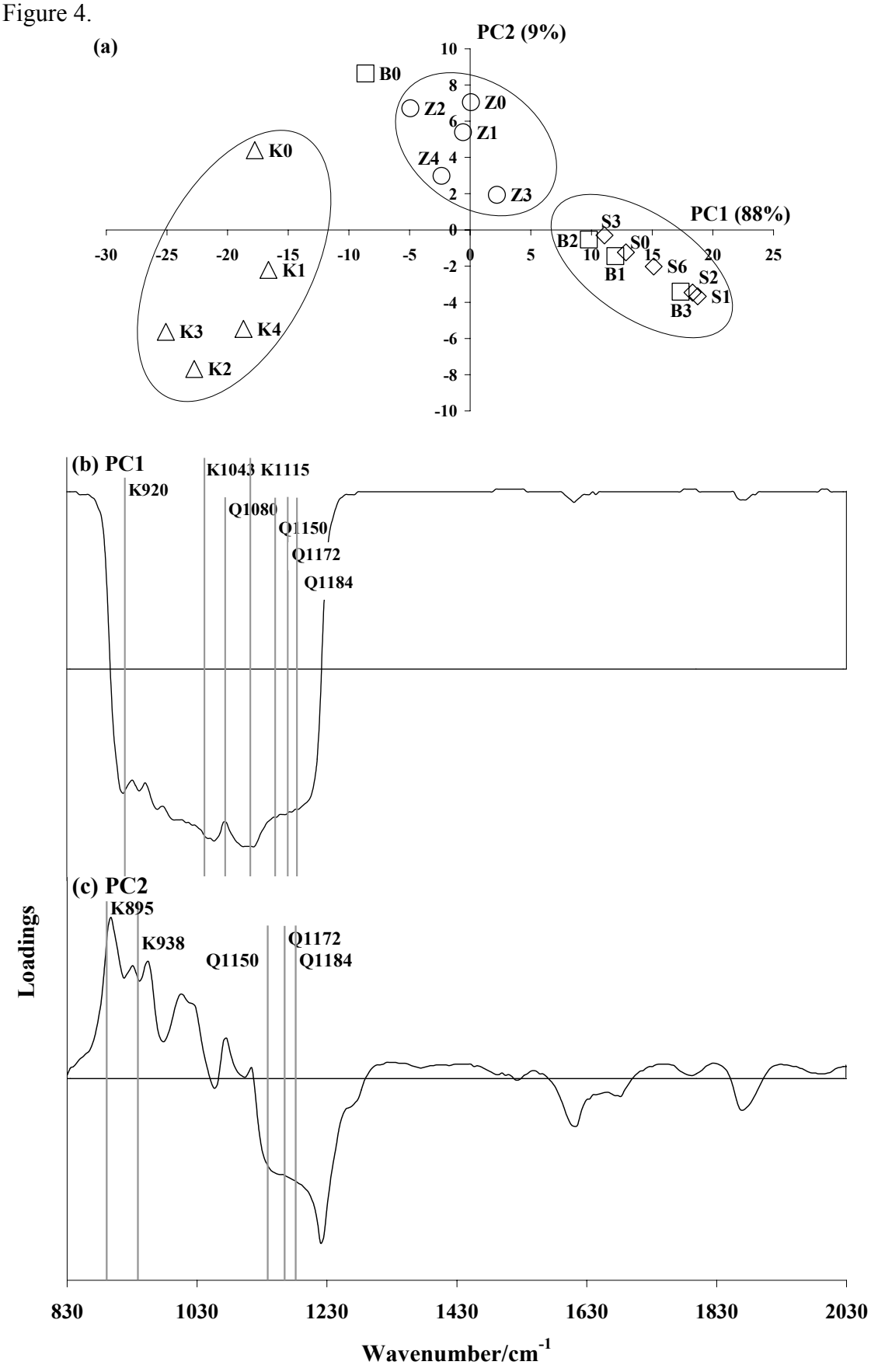
(a)
PC2 (9%)
PC1 (88%)
B0
Z2
Z0
Z1
Z4
Z3
K0
K1
K3
K4
K2
S3
B2
S0
B1
S6
S2
S1
B3
(b) PC1
K920
K1043 K1115
Q1080
Q1150
Q1172
Q1184
(c) PC2
K895
K938
Q1150
Q1172
Q1184
Loadings
830
1030
1230
1430
1630
1830
2030
Wavenumber/cm-1

Figure 5.

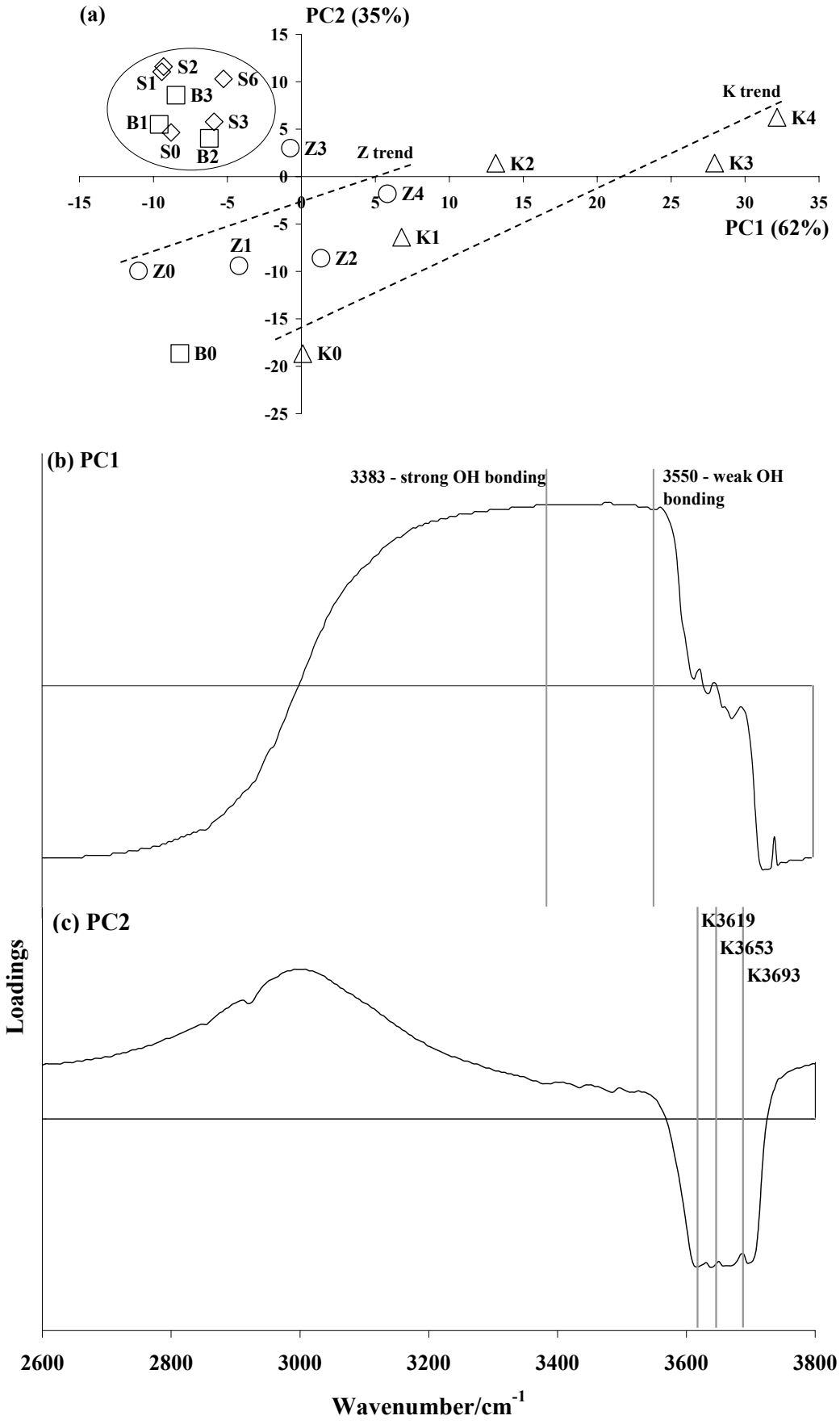
(a)
PC2 (35%)
PC1 (62%)
S1
S2
S6
B3
B1
S3
S0
B2
Z3
Z trend
K trend
K4
K2
K3
Z4
K1
Z1
Z2
Z0
B0
K0
(b) PC1
3383 - strong OH bonding
3550 - weak OH bonding
(c) PC2
K3619
K3653
K3693
Loadings
Wavenumber/cm-1

Figure 6.

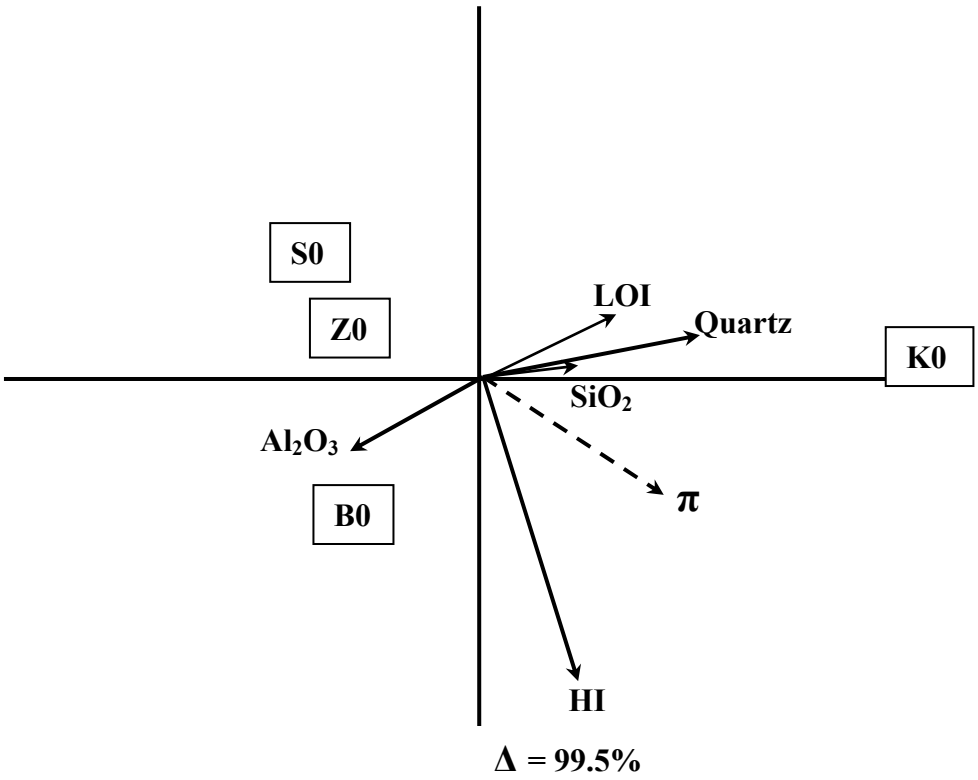

Figure 7.

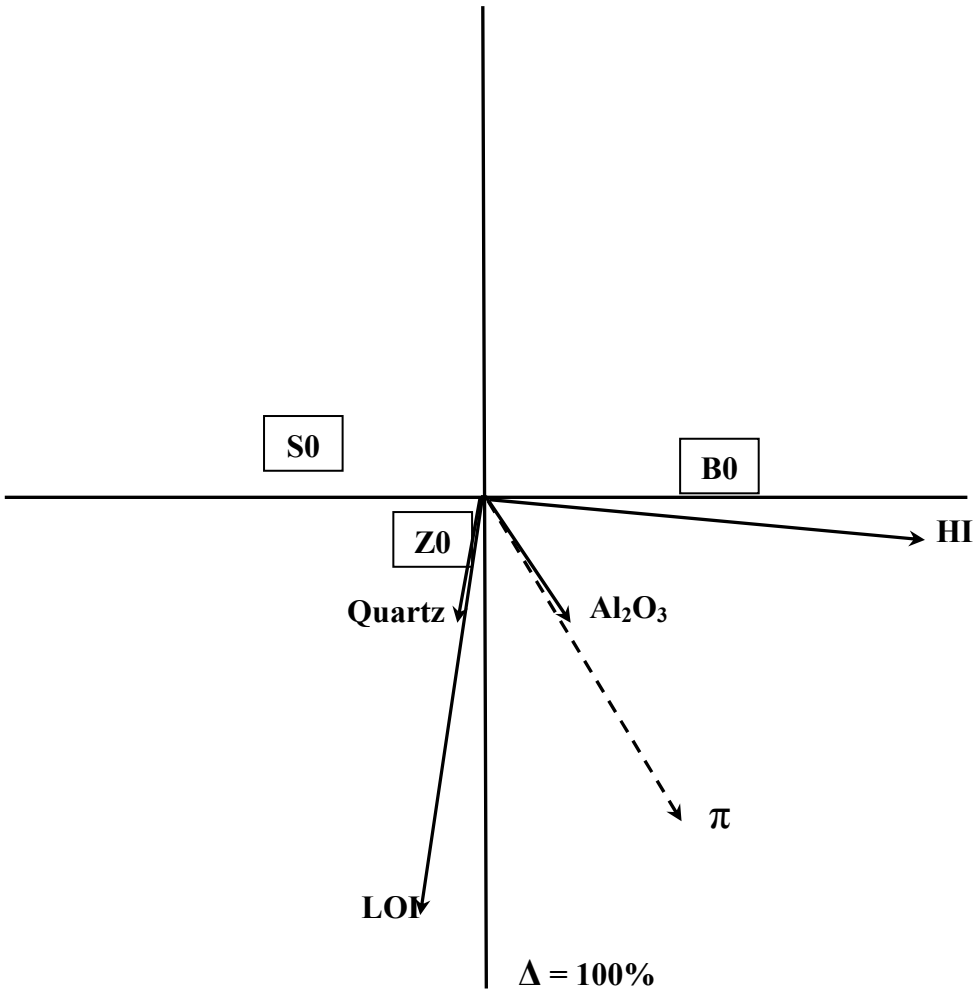

Figure 8.

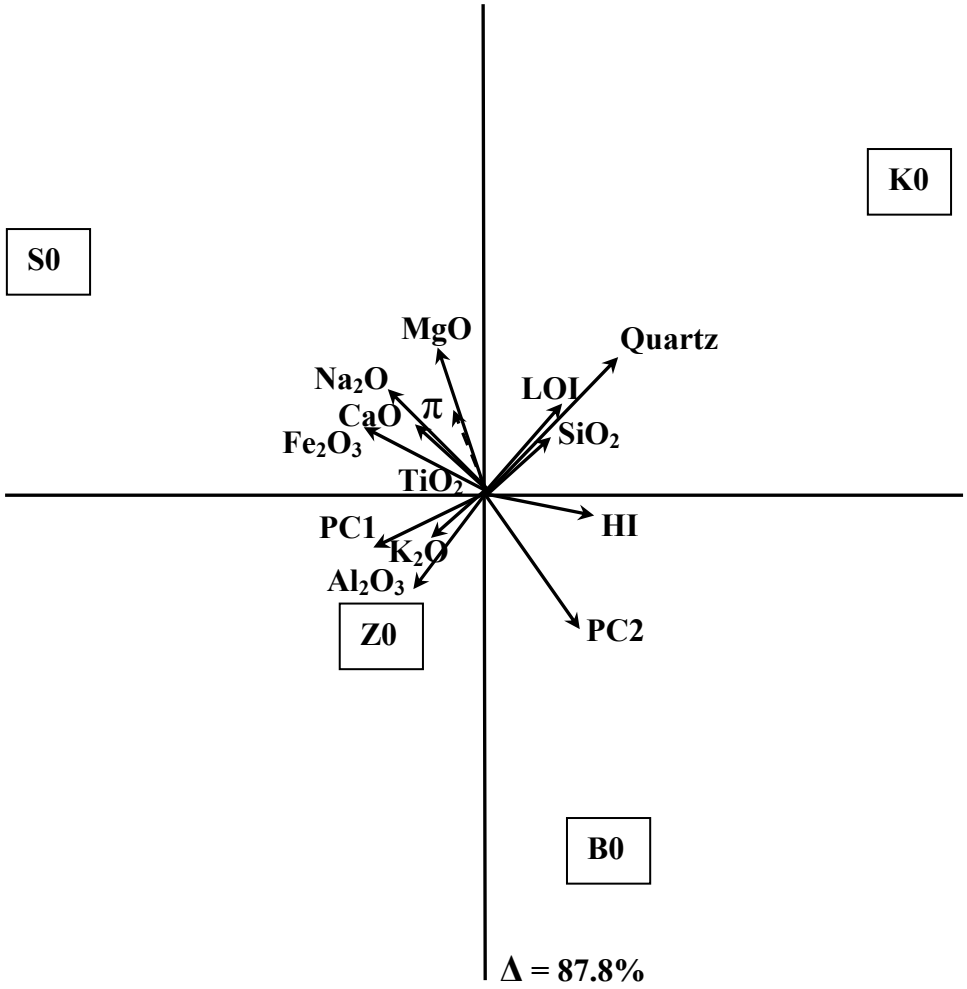
K0
S0
MgO
Quartz
Na2O
LOI
π
CaO
SiO2
Fe2O3
TiO2
PC1
HI
K2O
Al2O3
Z0
PC2
B0
Δ = 87.8%

Figure 9.

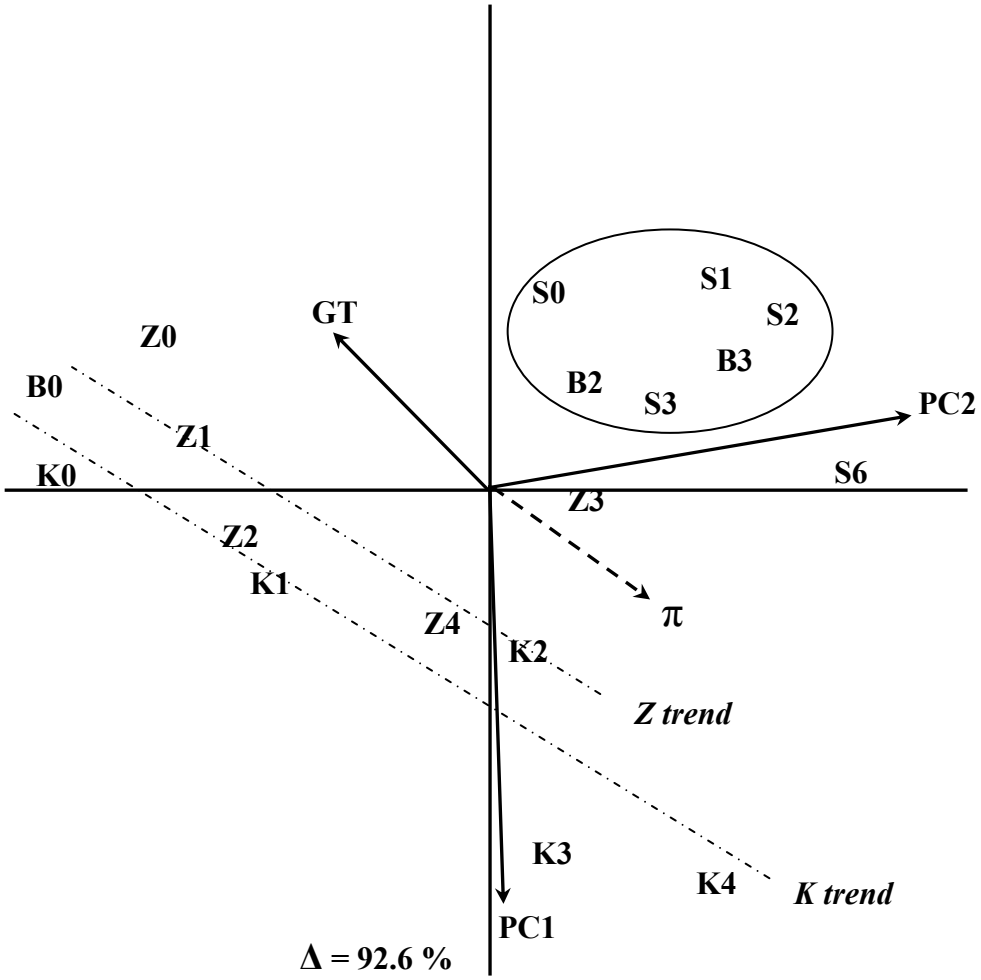
S0
S1
S2
B3
B2
S3
GT
Z0
B0
Z1
K0
PC2
S6
Z3
Z2
K1
π
Z4
K2
Z trend
K3
K4
K trend
PC1
Δ = 92.6 %